





Article

Controllable Connection of Fe_2Se_3 Double Chains and $\text{Fe}(\text{dien})_2$ Complexes for Organic–Inorganic Hybrid Ferrimagnet with a Large Coercivity

Xiaolei Shang^{1,2}, Xiaoling Men^{1,2}, Qifeng Kuang^{1,2}, Shaojie Li³, Da Li^{1,2,*}  and Zhidong Zhang¹ ¹ Shenyang National Laboratory for Materials Science, Institute of Metal Research, Chinese Academy of Sciences, 72 Wenhua Road, Shenyang 110016, China² School of Materials Science and Engineering, University of Science and Technology of China, 72 Wenhua Road, Shenyang 110016, China³ Instrumental Analysis and Research Center, Dalian University of Technology, Panjin 124221, China

* Correspondence: dali@imr.ac.cn; Tel.: +86-24-8397-8846

Abstract: Organic–inorganic hybrid materials built by inorganic and organic building units have attracted intensive interest in the past decades due to unique chemical and physical properties. However, rare organic–inorganic hybrid materials show excellent permanent magnetic properties. Here, we develop a facile chemical solution method to bottom-up synthesize a new hybrid $(\text{Fe}_2\text{Se}_3)_2[\text{Fe}(\text{dien})_2]_{0.9}$. This hybrid phase with the space group $P2_1/c$ (14) possesses a rodlike shape with a diameter of 100–2000 nm and a length of 5–50 μm . The hybrid rods are ferrimagnetic with a Curie temperature (T_C) of 11 K. They show a high coercivity (H_C) of 4.67 kOe and a saturation magnetization (M_S) of 13.5 emu/g at 2 K. Compared with orthorhombic $(\text{FeSe}_2)_2\text{Fe}(\text{dien})_2$, the excellent magnetic performance of the hybrid rods is ascribed to the monoclinic hybrid structure built by $\text{Fe}(\text{dien})_2$ complexes and Fe_2Se_3 double chains. Our study provides guidance for connecting inorganic fragments of FeSe_2 single chains, Fe_2Se_3 double chains or $\beta\text{-Fe}_3\text{Se}_4$ layers with $\text{Fe}(\text{dien})_2$ complexes for organic–inorganic hybrid phases with varied crystal structures and magnetic properties.



Citation: Shang, X.; Men, X.; Kuang, Q.; Li, S.; Li, D.; Zhang, Z. Controllable Connection of Fe_2Se_3 Double Chains and $\text{Fe}(\text{dien})_2$ Complexes for Organic–Inorganic Hybrid Ferrimagnet with a Large Coercivity. *Nanomaterials* **2023**, *13*, 487. <https://doi.org/10.3390/nano13030487>

Academic Editor: Vladimir Dubrovskii

Received: 25 December 2022

Revised: 16 January 2023

Accepted: 23 January 2023

Published: 25 January 2023



Copyright: © 2023 by the authors. Licensee MDPI, Basel, Switzerland. This article is an open access article distributed under the terms and conditions of the Creative Commons Attribution (CC BY) license (<https://creativecommons.org/licenses/by/4.0/>).

Keywords: organic–inorganic hybrid materials; chemical solution method; Fe_2Se_3 double chains; coercivity

1. Introduction

Over the past years, the development of organic magnetic materials has been intensively explored for both fundamental research and technological applications [1]. Organic–inorganic hybrid materials combining both organic and inorganic components exhibit diverse structures and unique physical and chemical properties. The advantages of organic–inorganic hybrid materials have attracted strong interest in potential applications in electronic and optical devices [2,3], protective coatings [4], catalysts [5], high-temperature superconductors [6], and so on. Many organic–inorganic hybrid materials are antiferromagnetic or weak ferromagnetic (ferrimagnetic) with low magnetic ordering temperatures [7–11]. Separation of magnetic inorganic fragments, such as one-dimensional (1D) chains [12,13] and 2D plates [14], by organic molecules or complexes results in the magnetism of organic–inorganic hybrid materials, and their magnetic ordering temperatures are usually much below room temperature [15–18]. Nevertheless, there are rare magnetic organic–inorganic hybrid materials, for example, $(\text{Fe}_2\text{Se}_3)_4[\text{Fe}(\text{tepa})]$ (tepa = tetraethylenepentamine) [19], $(\beta\text{-Fe}_3\text{Se}_4)_4[\text{Fe}(\text{teta})_{1.5}]$ (teta = triethylenetetramine) [20] and $(\text{NH}_3\text{-CH}_2\text{-C}_6\text{H}_4\text{CO}_2\text{H})[\text{SnCl}_6]$ [21], showing their magnetic ordering temperatures higher than room temperature. Moreover, Fe^{3+} vacancy doping gives rise to a room-temperature long-range ferrimagnetic (FIM) order in an organic–inorganic hybrid $(\text{FeSe}_2)_2\text{Fe}(\text{dien})_2$ (dien = diethylenetriamine) [22]. Noncompensated spins in the

$(\text{Fe}_{0.86}\text{Se}_2)_2\text{Fe}(\text{dien})_2$ due to Fe^{3+} vacancies are produced by controllable self-assemble of 1D FeSe_2 short chains and $\text{Fe}(\text{dien})_2$ complexes [22], which is different from the “chemical scissors” model to bond isolated single FeSe_2 chains with $\text{Fe}(\text{dien})_2$ complexes [13,17]. Moreover, most organic–inorganic hybrid materials have low coercivities. It is very difficult to improve coercivity for organic and inorganic hybrid materials. It is preferable to control the stoichiometry of the inorganic component and the combination of inorganic and organic fragments for excellent magnetic performance. From the point of view of magnetism, it is necessary to develop a “bottom-up self-assemble” that is able to enhance the magnetic properties of organic–inorganic hybrid materials through tuning magnetic interactions between Fe-amine complexes and Fe_xSe building blocks in different dimensions [23]. In comparison with a “top-down” method to synthesize organic–inorganic hybrid materials [24], the “bottom-up self-assemble” is more conducive to manipulating the assemble process at the atomic/molecular level. Recently, quasi-1D spin-ladder compounds, $M\text{Fe}_2\text{Se}_3$ ($M = \text{Ba}, \text{Cs}$), have attracted considerable interest [25–28], in which iron and selenium form Fe_2Se_3 double chains. FeSe_4 tetrahedra sharing edges in Fe_2Se_3 double chains are much different from the FeSe_2 single chains mentioned above. More recently, we reported a new type of iron chalcogenide-based superconducting system, which originates from a suppression of the long-range FIM order of a parent phase, $[\text{Fe}(\text{tepa})](\beta\text{-Fe}_2\text{Se}_3)_4$, through simultaneously tuning the host and the spacer layers [29].

In this work, we report a facile solution-based synthetic route to fabricate a new organic–inorganic hybrid magnet built by organic $\text{Fe}(\text{dien})_2$ and inorganic Fe_2Se_3 double chains. The $(\text{Fe}_2\text{Se}_3)_2[\text{Fe}(\text{dien})_2]_{0.9}$ hybrid forms with a rodlike shape, which is a single phase in a monoclinic crystal structure with the space group $P2_1/c$ (14). Temperature dependence of magnetization reveals the ferrimagnetism of the $(\text{Fe}_2\text{Se}_3)_2[\text{Fe}(\text{dien})_2]_{0.9}$ rods with the Curie temperature (T_C) of 11 K. The coercivity (H_C) and saturation magnetization (M_S) of the $(\text{Fe}_2\text{Se}_3)_2[\text{Fe}(\text{dien})_2]_{0.9}$ magnet is 4.67 kOe and 13.5 emu/g, respectively, at 2 K. Our study not only provides guidance for developing a chemical solution method for controllable fabrication of a new type of organic–inorganic hybrid materials but also extends a potential application as an organic permanent magnet due to high coercivity of this organic–inorganic hybrid magnet.

2. Materials and Methods

2.1. Chemicals

Iron(III) acetylacetonate $[\text{Fe}(\text{acac})_3]$, 98% was purchased from Aladdin reagent company (Shanghai, China). Diethylenetriamine (dien, 99%), acetone (99.7%), and isopropyl alcohol (99.7%) were purchased from Sinopharm Chemical Reagent Co., Ltd. (Shenyang, China). Se powder (99.99%) was purchased from Macklin Biochemical Co., Ltd. (Shanghai, China). All chemicals were used without further purification.

2.2. Synthesis of Monoclinic $(\text{Fe}_2\text{Se}_3)_2[\text{Fe}(\text{dien})_2]_{0.9}$ Nanorods

In a typical synthesis of $(\text{Fe}_2\text{Se}_3)_2[\text{Fe}(\text{dien})_2]$ hybrid nanorods, 3.25 mmol $\text{Fe}(\text{acac})_3$, 4 mmol Se powder and 40 mL dien were mixed into a 100 mL quartz crucible in a stainless-steel autoclave under magnetic stirring throughout the entire reaction process. Under an argon gas flow, the mixture was kept at room temperature for 1 h, and then was heated to 393 K and kept at this temperature for 1 h to remove moisture and oxygen. Then the temperature was raised to 433 K and kept for 3 h in order that all raw materials were dissolved into the solution. The solution was subsequently heated to 503 K at a rate of $0.4 \text{ K} \cdot \text{min}^{-1}$ and maintained for 3 days. At room temperature, the product was centrifuged at 8000 rpm for 5 min. A ThermoFisher inductively coupled plasma (ICP) spectroscopy gave a concentration of 0.0072 and 0.06 mg mL^{-1} , respectively, for Fe and Se ions left in the light-yellow transparent supernatant above the precipitate, suggesting that all the Fe and Se atoms in the starting materials were combined in the hybrid product. The precipitate was washed by 20 mL acetone and 5 mL isopropyl alcohol the first time and then rewashed in 20 mL acetone four times. The product was dried in a vacuum for further characterization.

For comparison, $\text{Fe}_3\text{Se}_4(\text{dien})_2$ particles and $(\text{Fe}_{3.5}\text{Se}_4)\text{-dien}$ plates were synthesized in a manner similar to the synthesis of monoclinic $(\text{Fe}_2\text{Se}_3)_2[\text{Fe}(\text{dien})_2]_{0.9}$ rods except that the reaction temperature was set to 473 K and 513 K, respectively. The Fe:Se stoichiometry for different hybrid material was determined by the amounts of the Fe and Se precursors. However, a formula of the hybrid plates cannot be determined due to the hybrid phase being mixed with some decomposed tetragonal Fe_xSe .

2.3. Characterization

Powder X-ray diffraction (XRD) was performed on a Rigaku D/Max-2400 diffractometer (Rigaku Inc., Tokyo, Japan) with a $\text{Cu K}\alpha$ radiation source ($\lambda = 0.154056$ nm). The software Fullprof was used to refine the structure of the hybrid product. The size, morphology and microstructure of the as-synthesized products were observed by a JSM 6301F field-emission scanning electronic microscope (SEM) (JEOL Inc., Japan) and a Tecnai G2 F20 transmission electronic microscope (TEM) (FEI Inc., Hillsboro, OR, USA) at 200 kV. The elemental compositions of products were determined by Oxford X-ray energy dispersive (EDX) spectroscopy and inductively coupling plasma spectrometry (ICP). Fourier transform infrared (FTIR) spectrum was recorded on a Nicolet iN10 MX & iS10 spectrometer using the KBr pellet technique (Thermo Fisher Inc., Waltham, MA, USA). Thermal gravimetric analysis (TGA) was performed on an STA6000 thermal analyzer (PerkinElmer Inc., Waltham, MA, USA) under N_2 flow with a heating rate of $10\text{ K}\cdot\text{min}^{-1}$ between 300 and 800 K. Fe *L*-edge X-ray absorption spectroscopy (XAS) measurements were performed at Beamline 08U1A of the Shanghai Synchrotron Radiation Facility (SSRF) in total electron yield (TEY) mode at room temperature. Magnetic hysteresis loops and temperature-dependent magnetization in the field-cooling (FC) mode (at $H = 100$ Oe) were carried out using a superconducting quantum interference device (SQUID) (Quantum Design Inc., San Diego, CA, USA).

3. Results

3.1. Structural Properties

SEM (Figure 1a,b) and TEM (Figure 1d) images illustrate that the hybrid product synthesized at 503 K for 3 days possesses a rodlike shape with a size distribution of about 100–2000 nm for diameter and 5–50 μm for length. The microstructure at the edge of a rod with a large diameter reveals cleavage grooves (Figure 1b), suggesting that the hybrid nanorods with smaller diameters are cleaved down from the rods with large diameters. The selected area electron diffraction (SAED) pattern of a hybrid nanorod in the inset of Figure 1d reveals periodic crystal structure along the longitudinal direction. Compared with the previous iron vacancy doped hybrids [22], clear diffraction points in the SAED pattern show a single crystal feature of the hybrid nanorod, possibly due to the absence of iron vacancies in the hybrid rods. This was supported by the composition analyses. The EDX spectrum as shown in the inset of Figure 1c indicates the presence of Fe, Se, C and N elements, and Fe and Se are the only heavy elements in the hybrid rods. Elemental mapping of a single nanorod (Figure 1e) shows the even distribution of Fe, Se, C, and N in the hybrid rod (Figure 1f–i). The relative molar ratio of Fe to Se in the hybrid rods was determined to be 44.84/55.16 (3.25/4) by EDX, very similar to the value of 3.27/4 determined by the ICP technique. The FTIR spectrum (Figure 2) presents characteristic peaks of dien featured by the vibration bands of $-\text{CH}_2-$, $-\text{NH}_2$, and $-\text{NH}$. It reveals the incorporation of organic dien molecules in the hybrid structure. Similar to the previous iron vacancy doped hybrids [22], the bands of $-\text{NH}_2$ shift from 3360 cm^{-1} for the asymmetric stretching vibration of free dien molecules to 3289 cm^{-1} for that of the hybrid rods and from 3280 cm^{-1} for the symmetric stretching vibration of free dien molecules to 3217 cm^{-1} for that of the hybrid rods, which correspond to the chemical coordination of $-\text{NH}_2$ groups with Fe^{2+} ions in the present hybrid rods.

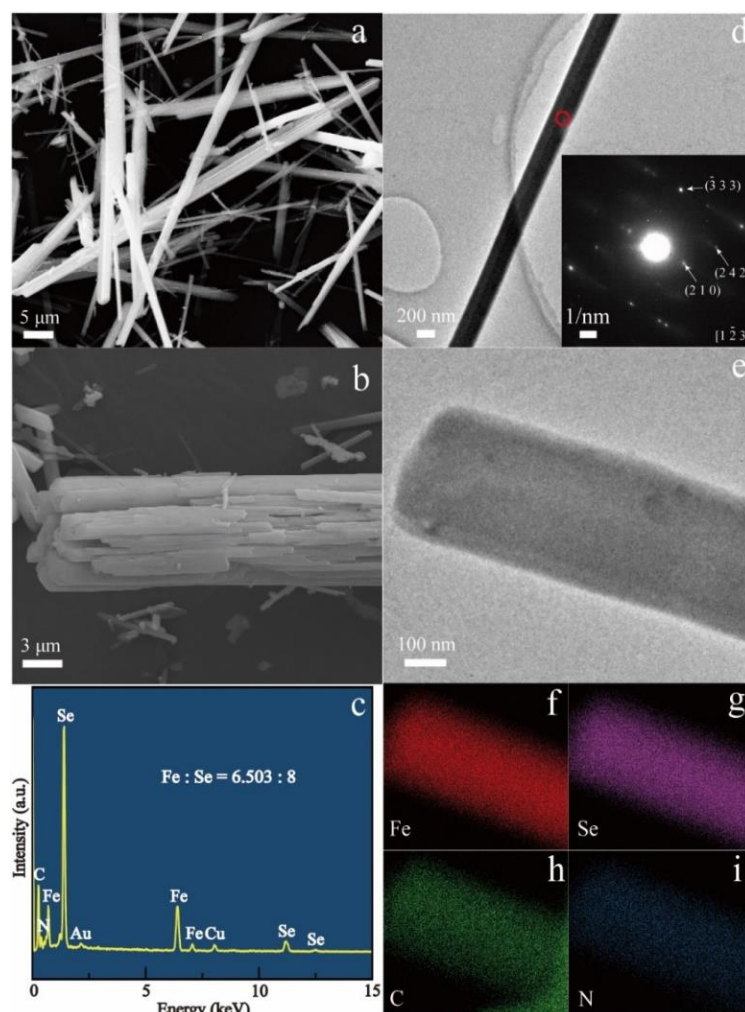


Figure 1. (a,b) SEM images and (c) the corresponding EDX spectrum of the $(\text{Fe}_2\text{Se}_3)_2[\text{Fe}(\text{dien})_2]_{0.9}$ hybrid rods. (d) Typical TEM image of a single hybrid rod. Inset shows the corresponding SAED pattern. (e) A STEM image and corresponding element mapping of (f) Fe, (g) Se, (h) C and (i) N for a single $(\text{Fe}_2\text{Se}_3)_2[\text{Fe}(\text{dien})_2]_{0.9}$ hybrid rod.

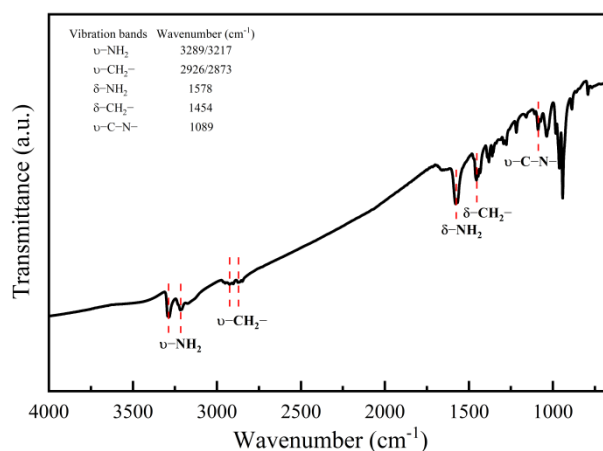


Figure 2. FTIR spectrum of the $(\text{Fe}_2\text{Se}_3)_2[\text{Fe}(\text{dien})_2]_{0.9}$ hybrid rods. The inset shows the vibration bands of $-\text{CH}_2-$, $-\text{NH}_2$, and $-\text{CN}-$.

TGA and dWeight/dT curves in Figure 3 show a weight loss (~6.7 wt%) from room temperature to the onset decomposition temperature (T_{onset}) ~540 K due to a small amount

of free dien and other organic solvents absorbed on the surface of the hybrid rods. The T_{onset} value is obviously higher than that of the previously reported $(\text{Fe}_{0.86}\text{Se}_2)_2\text{Fe}(\text{dien})_2$ [22]. Between 540 K and ~585 K, a sharp weight loss of about 15.9 wt% should be ascribed to releasing the bonded dien from the hybrid rods, while a slow weight loss (5.3 wt%) between 585 K and the end temperature (T_{end}) of ~700 K is due to the loss of the left dien and a small amount of Se. To obtain a precise content of dien in the hybrid rods, we performed the experiments as follows: At first, clean Al_2O_3 crucibles were calcined to 1100 K for 24 h in an air atmosphere. The Al_2O_3 crucibles were used to contain the hybrid rods for the subsequent thermal decomposition. The masses of an Al_2O_3 crucible and the hybrid rods were weighed together at different steps. The mass of the Al_2O_3 crucible was deducted for convenience. The hybrid rods with an initial mass of 68.6 mg were slowly heated to 580 K in an Ar flow for 24 h, at which temperature the hybrid rods were completely decomposed through releasing coordinated dien but without losing Se atoms from the decomposed product. The mass of the decomposition product was 51.1 mg. Therefore, the weight loss was determined to be about 25.4 wt%, which is smaller than the total weight loss obtained by TGA without loss of Se. If we subtract the loss of free dien and other organic solvents absorbed on the surface of the hybrid rods, the loss of coordinated dien should be about 18.7 wt%. Taking into account that there are 18.7 g of dien and 74.6 g of inorganic $\text{Fe}_{3.25}\text{Se}_4$ in 100 g of hybrid rods, the molar ratio y between dien to $\text{Fe}_{3.25}\text{Se}_4$ in the hybrid rods could be calculated by the equation:

$$y = \frac{18.7 / M_{\text{dien}}}{74.6 / M_{\text{Fe}_{3.25}\text{Se}_4}},$$

where M_{dien} and $M_{\text{Fe}_{3.25}\text{Se}_4}$ are the molecular weights of the organic component (dien) and the inorganic component ($\text{Fe}_{3.25}\text{Se}_4$), respectively. The y for the hybrid rods is ~1.2 and the formula of the hybrid rods is determined as $(\text{Fe}_{3.25}\text{Se}_4)(\text{dien})_{1.2}$.

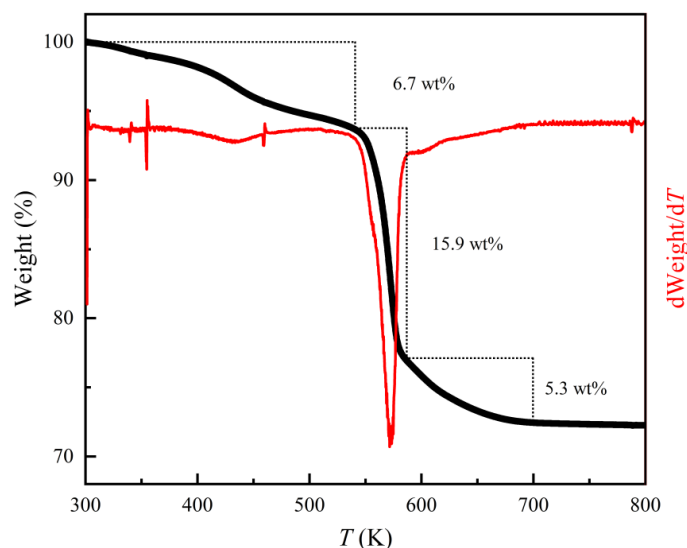


Figure 3. TGA and dWeight/dT curves of the $(\text{Fe}_2\text{Se}_3)_2[\text{Fe}(\text{dien})_2]_{0.9}$ hybrid rods.

Powder XRD pattern of the hybrid rods (Figure 4) reveals that all Bragg diffraction peaks can be refined and indexed by using the monoclinic structure with the space group $P2_1/c$ (14). The corresponding refinement process gave good R factors ($R_p = 8.52\%$, $R_{wp} = 7.45\%$ and $\chi^2 = 2.72$), and refined room-temperature lattice parameters of the hybrid material are $a = 11.397(7)$ Å, $b = 19.376(3)$ Å, $c = 11.185(6)$ Å and $\beta = 105.04^\circ$. The crystal structure of the hybrid rods is the same as that for $\text{Fe}_3\text{Se}_4(\text{tren})$ ($\text{tren} = \text{tris}(2\text{-aminoethyl})\text{amine}$) [13] but different from those for previous orthorhombic $\text{Fe}_3\text{Se}_4(\text{dien})_2$ [13] and iron vacancy doped $(\text{Fe}_{0.86}\text{Se}_2)_2\text{Fe}(\text{dien})_2$ [22], in which two independent subsystems have been identified: 1D FeSe_2 chains and $\text{Fe}(\text{dien})_2$ complex. Because two dien molecules with six nitrogen atoms have bonded well with a Fe^{2+} to form a $[\text{Fe}(\text{dien})]^{2+}$

complex, the $\text{Fe}(\text{dien})_2$ complex should be the only organic fragment for the orthorhombic $\text{Fe}_3\text{Se}_4(\text{dien})_2$ [13] and the monoclinic hybrid rods. Therefore, a change of crystal structure from the orthorhombic $\text{Fe}_3\text{Se}_4(\text{dien})_2$ [13] to the present monoclinic hybrid rods should be ascribed to a bit increase of Fe atoms in the inorganic fragment of hybrid rods. The Fe_2Se_3 superstructure is the closest fragment to FeSe_2 in chemical composition [23]. Therefore, a formula of the hybrid rods may be written as $(\text{Fe}_{1.99}\text{Se}_3)_2[\text{Fe}(\text{dien})_2]_{0.9}$. Taking into account two independent subsystems consisting of the $(\text{Fe}_2\text{Se}_3)^{2-}$ double chains and the $\text{Fe}^{2+}(\text{dien})_2$ complexes, there are both Fe^{3+} and Fe^{2+} ions in the hybrid rods similar to the case of the orthorhombic $\text{Fe}_3\text{Se}_4(\text{dien})_2$ [13]. Figure 5 represents the Fe L -edge X-ray absorption spectrum (XAS) line of the monoclinic hybrid rods in total electron yield (TEY) mode, along with that of commercial Fe_3O_4 as a reference for Fe^{3+} and Fe^{2+} oxidation states. As a guide to the valence states, the line shapes of the sample are compared with that of reference, indicating the signatures of Fe^{3+} and Fe^{2+} . This reveals that there are both trivalent and bivalent Fe ions in the as-synthesized monoclinic hybrid rods. It should be noted that information on the monoclinic hybrid phase was seldom mentioned in the previous transition-metal chalcogenides-dien systems [13,17,20,22,30–33].

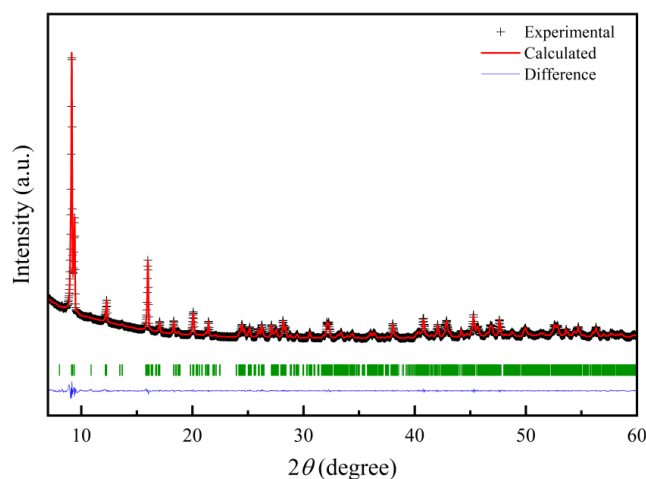


Figure 4. Powder XRD pattern of $(\text{Fe}_2\text{Se}_3)_2[\text{Fe}(\text{dien})_2]_{0.9}$ hybrid rods recorded at room temperature (solid crosses) with Rietveld refinements and difference curves.

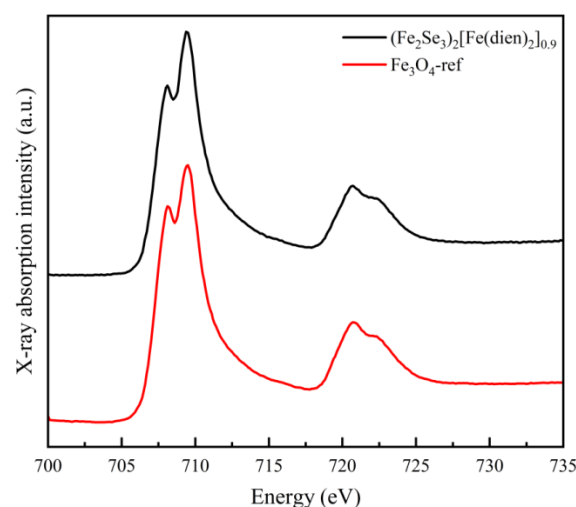


Figure 5. XAS of the $(\text{Fe}_2\text{Se}_3)_2[\text{Fe}(\text{dien})_2]_{0.9}$ hybrid rods and Fe_3O_4 as reference. The main peak of Fe L_3 -absorption edge is at 710 eV with lower shoulder at 708 eV, and the main peak of Fe L_2 -absorption edge is at 720 eV with higher shoulder at 722 eV.

3.2. Growth Mechanism

Similar to the Fe vacancies doped orthorhombic hybrid cuboids [22], the monoclinic hybrid rods have been synthesized by using soluble iron and selenium precursors and organic dien. Although inorganic FeSe_x building blocks, such as 1D FeSe_2 chains and 2D $\beta\text{-Fe}_3\text{Se}_4$ layers, play an important role in the formation of the FeSe_x -amine hybrid materials [13,17,20,22], there is no precise information on how the 1D FeSe_2 chains change to the 2D $\beta\text{-Fe}_3\text{Se}_4$ layers. In the solution syntheses, the dien molecules should play three important roles in the solvent, the reductive agent and the precursor at the same time [22]. Se atoms and a part of Fe^{3+} ions can be reduced by dien to Se^{2-} ions and Fe^{2+} ions, respectively. Meanwhile, the redox reactions produce nitrogen, serving as the production of the oxidation [21,34]. Based on a bottom-up growth mechanism, Figure 6 illustrates three combination modes of organic $\text{Fe}(\text{dien})_2$ complexes with (I) 1D FeSe_2 chains, (II) Fe_2Se_3 double chains and (III) 2D $\beta\text{-Fe}_3\text{Se}_4$ layers, respectively, in the present reaction system, following the reaction formulas:

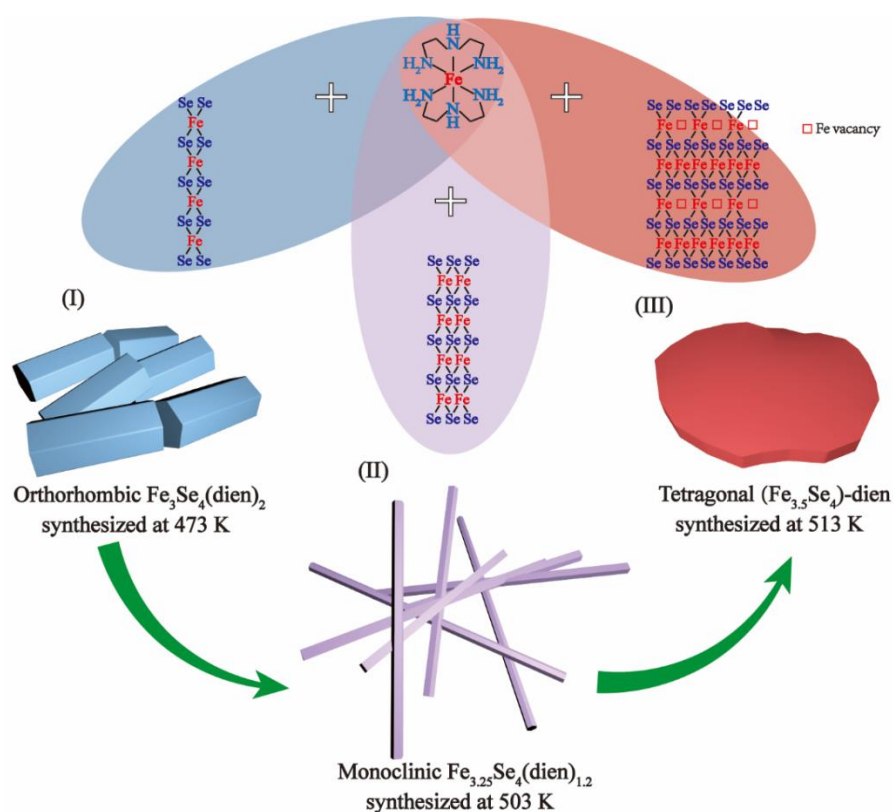


Figure 6. Schematic illustration of combining organic $\text{Fe}(\text{dien})_2$ complexes with (I) 1D FeSe_2 chains, (II) Fe_2Se_3 double chains and (III) 2D Fe_xSe layers, respectively, for the syntheses of three hybrid phases at different reaction conditions.

The $\text{Fe}^{2+}(\text{dien})_2$ complexes are formed by coordinating the Fe^{2+} ions with dien molecules, while the FeSe_2 chains are initially created by the reaction of Se^{2-} and Fe^{3+} ions, following the reaction formulas (1) and (2). Combinations of FeSe_2 chains and $\text{Fe}^{2+}(\text{dien})_2$ complexes are driven by the $\text{Se}\cdots\text{H-N}$ interactions due to strong electronegativity of Se atoms [22].

Therefore, the synthesis of orthorhombic $[\text{FeSe}_2]_2[\text{Fe}(\text{dien})_2]$ with a cuboid shape can be proposed as the growth model (I) through a self-assembly reaction of 1D FeSe_2 chains and $\text{Fe}^{2+}(\text{dien})_2$ complexes following the reaction formula (3). The powder XRD pattern of the hybrid cuboids (Figure 7a) indicates that all Bragg diffraction peaks can be refined and indexed by using the orthorhombic structure with the space group $C2221$ (No. 20). Such an XRD pattern reveals the same crystal structure as that of $\text{Fe}_3\text{Se}_4(\text{dien})_2$ [13]. The corresponding refinement process gave good R factors ($R_p = 18.3\%$, $R_{wp} = 18.7\%$ and $\chi^2 = 6.48$) for the hybrid cuboids. Refined lattice parameters at room temperature of the hybrid cuboids are $9.226(6)$ Å for a axis, $18.000(0)$ Å for b axis, and $11.610(7)$ Å for c axis, about 0.94% and 0.58% expansion along the a and c axes and 0.67% shrinkage along the b axis when compared with those of $\text{Fe}_3\text{Se}_4(\text{dien})_2$ [13]. The orthorhombic hybrid particles are in the paramagnetism in good agreement with previous $\text{Fe}_3\text{Se}_4(\text{dien})_2$ [13]. The magnetic properties are not shown here.

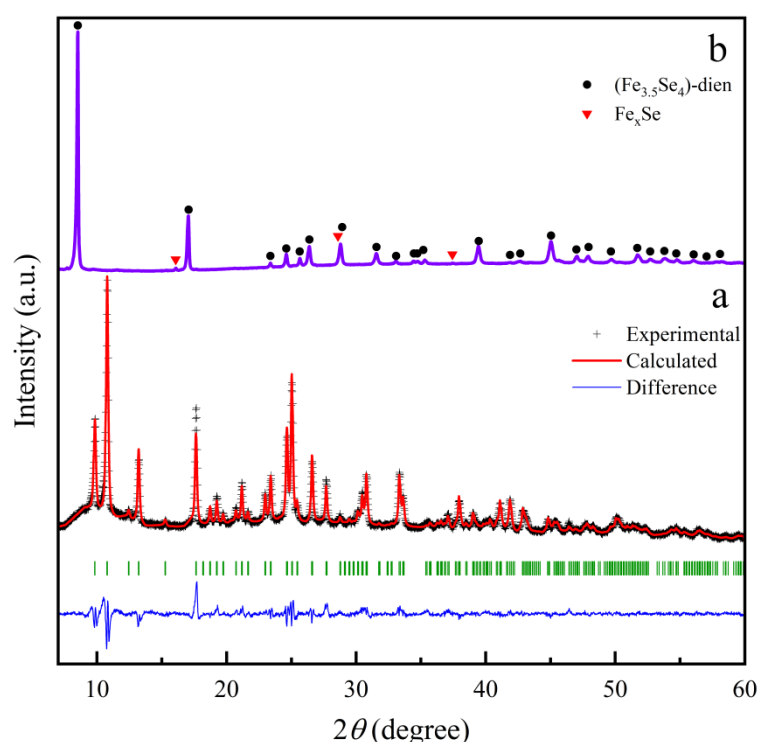


Figure 7. Powder XRD patterns of (a) $[\text{FeSe}_2]_2[\text{Fe}(\text{dien})_2]$ particles and (b) $(\text{Fe}_{3.5}\text{Se}_4)\text{-dien}$ plates.

Given the redox reaction system at a higher temperature (503 K), Fe^{3+} ions are preferably reduced to Fe^{2+} ions. When the molar ratio of Fe and Se atoms in the starting materials changes from 3:4 to 3.25:4, a diffusion of more iron atoms into the orthorhombic $[\text{FeSe}_2]_2[\text{Fe}(\text{dien})_2]$ would occur following the reaction formula (4), resulting in the monoclinic hybrid rods (Figure 4). A reasonable molecular formula for the hybrid rods is proposed as $[\text{Fe}_{1.125}^{3+}\text{Fe}_{0.875}^{2+}\text{Se}_3^{2-}]_2[\text{Fe}^{2+}(\text{dien})_{0.875}]$ according to electrical neutrality principles. The content of 0.875 dien/cell is obtained by balancing chemical Equation (4), which is almost the same as the experimental value of 0.9 dien/cell for the present hybrid rods determined above. Assuming that the small difference between the calculated and the experimental values is in range of the analytical error, we propose that the monoclinic hybrid rods are built by Fe_2Se_3 double chains and $\text{Fe}(\text{dien})_2$ complexes in the model (II).

Moreover, further increases in the molar ratio of Fe and Se to 3.5:4 and the reaction temperature to 513 K result in the hybrid nanoplates. Figure 8 shows the morphology transformation from particles for the orthorhombic phase to rods for the monoclinic phase and plates for the $(\text{Fe}_{3.5}\text{Se}_4)\text{-dien}$. Figure 7b presents the XRD pattern of $(\text{Fe}_{3.5}\text{Se}_4)\text{-dien}$ hybrid plates. Two strong peaks at low 2θ angles of 8.48° and 17.00° with lattice spacings of

10.42 and 5.21 Å reveal the presence of period inorganic layers separated by the $\text{Fe}(\text{dien})_2$ complex, similar to previous hybrid plates with a tetragonal $\beta\text{-Fe}_3\text{Se}_4$ superstructure [20] and an inorganic $\text{Fe}_{0.9}\text{Co}_{0.1}\text{S}_{1.2}$ unit [31]. Because the hybrid plates are mixed by an impurity of Fe_xSe with an uncertain quality, the formula for the hybrid phase is not determined by the same method for the hybrid rods. However, an ordered tetragonal superstructure is determined in the presence of the hybrid plates by a SAED image (the inset of Figure 8d), which is similar to that of the inorganic $\text{Fe}_{0.9}\text{Co}_{0.1}\text{S}_{1.2}$ unit [31] and the tetragonal $\beta\text{-Fe}_3\text{Se}_4$ superstructure [20]. Taking into account the composition, this ordered superstructure is suggested as the tetragonal $\beta\text{-Fe}_3\text{Se}_4$. Therefore, the growth model (III) can be illustrated by the combination of the inorganic tetragonal $\beta\text{-Fe}_3\text{Se}_4$ superstructures and the $\text{Fe}(\text{dien})_2$ complexes for the synthesis of hybrid nanoplates in the iron selenide-dien hybrid system. Efforts to examine the crystal structure of $(\text{Fe}_{3.5}\text{Se}_4)\text{-dien}$ hybrid plates are currently in progress.

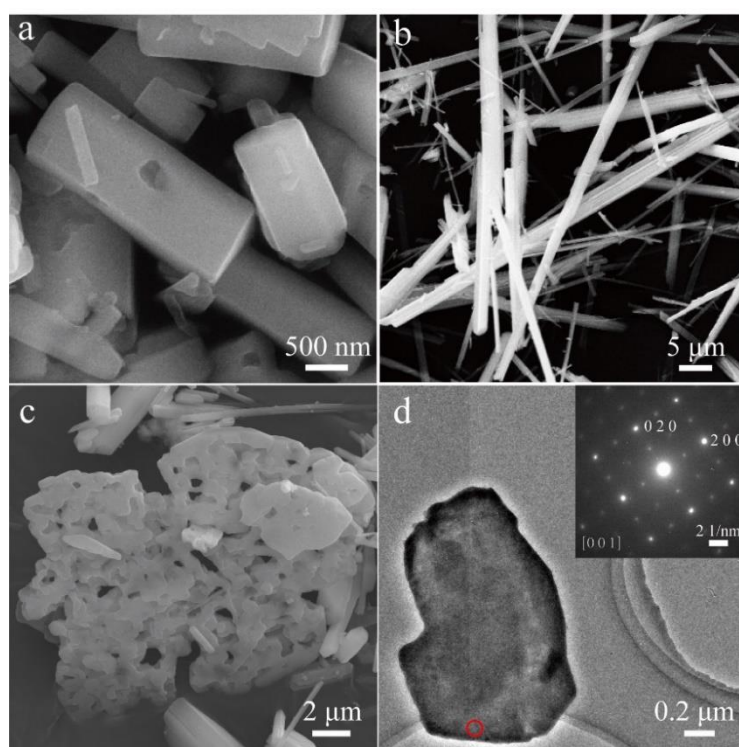


Figure 8. Microstructure of (a) $[\text{FeSe}_2]_2[\text{Fe}(\text{dien})_2]$ hybrid particles, (b) $(\text{Fe}_2\text{Se}_3)_2[\text{Fe}(\text{dien})_2]_{0.9}$ hybrid rods, (c) an intermediate product between the rodlike and the platelike samples and (d) a $(\text{Fe}_{3.5}\text{Se}_4)\text{-dien}$ hybrid plate. Inset shows the corresponding SAED pattern obtained perpendicular to the nanoplate marked by the red circle.

As shown in Figure 6, varied inorganic building units are key factors for syntheses of corresponding hybrid products, which depend on the Fe/Se stoichiometry and the reacting temperatures. In the solution reaction system, iron-diffusion reactions, such as the reaction formulas (3) and (4), are driven by different reaction temperatures. Figure 4 reveals a single phase of hybrid rods with a monoclinic structure, which is built by Fe_2Se_3 double chains and $\text{Fe}(\text{dien})_2$ complexes at a molecular level and in a controllable manner. An improper reaction condition will result in mixtures of several hybrid materials but not a single phase.

3.3. Magnetic Properties

Figure 9 represents the magnetic properties of the monoclinic hybrid rods. In contrast to the stoichiometric $[\text{FeSe}_2]_2[\text{Fe}(\text{dien})_2]$ that is paramagnetic [13], the temperature dependence of the magnetization in the FC process for the monoclinic hybrid rods shows a magnetic transition at the Curie temperature (T_C) of 11 K (inset of Figure 9). The T_C

value is determined by the point of intersection of the two tangents around the inflection point of the FC magnetization curve. Such a T_C value is much lower than that of the iron vacancy doped $(\text{Fe}_{0.86}\text{Se}_2)_2\text{Fe}(\text{dien})_2$ [22], revealing that the ferrimagnetism is independent on the uncompensated magnetic iron ions. There is no magnetic transition above 11 K, suggesting that the origin of ferrimagnetic behavior of this hybrid material could not be caused by traces of ferromagnetic impurity Fe_3O_4 with the T_C of about 860 K and ferromagnetic iron selenides, such as Fe_3Se_4 and Fe_7Se_8 . It is well known that the T_C values for Fe_3Se_4 and Fe_7Se_8 are about 320 K [35] and 450 K [36], respectively. The magnetic hysteresis loops of the hybrid rods in Figure 9 further exhibit the ferromagnetic feature in a temperature ranging from 2 to 10 K. The magnetization at 50 kOe (M_{50}) and coercivity of the hybrid rods are 13.6 emu/g and 4.67 kOe, respectively, at 2 K. Such a M_{50} of the hybrid rods is obviously larger than the saturation magnetization value of 5.6 emu/g for ferromagnetic $(\text{CH}_3\text{NH}_3)_2\text{CuCl}_4$ at 10 K [7], of 6 emu/g for FIM $[\text{Fe}_{14}\text{Se}_{16}](\text{tapa})$ hybrid plates at 10 K [29] and 0.01 emu/g for $(\text{NH}_3\text{--CH}_2\text{--C}_6\text{H}_4\text{CO}_2\text{H})[\text{SnCl}_6]$ at 300 K [21]. Moreover, the high coercivity of the hybrid rods is rare in organic–inorganic hybrid materials, for example, 30 Oe for the $(\text{PEA})_2\text{CuCl}_4$ ($\text{PEA} = \text{C}_6\text{H}_5\text{C}_2\text{H}_4\text{NH}_3$) film at 5 K [9], 404 Oe for the $(\text{NH}_3\text{--CH}_2\text{--C}_6\text{H}_4\text{CO}_2\text{H})[\text{SnCl}_6]$ at 300 K [21], 1.5 kOe for TBA intercalated NiPS_3 (TBA = tetrabutylammonium) at 5 K and 2.2 kOe for cobaltocenium ions $(\text{Co}(\text{Cp})_2)^+$ ($\text{Cp} = \text{cyclopentadienyl ring } \text{C}_5\text{H}_5^-$) intercalated NiPS_3 at 5 K [24]. We suggest that the large coercivity results from large uniaxial magnetocrystalline anisotropy of the hybrid rods [37]. As the temperature rises, the coercivity significantly decreases to 1.65 kOe at 5 K and about 20 Oe at 10 K. It is obvious that the magnetic field dependence of magnetization is in the ferromagnetic characteristics in a low magnetic field range, but in a linear magnetization in the high magnetic field range. The linear magnetization curves in the high field range may indicate the existence of a paramagnetic or antiferromagnetic component because of the nonsaturation feature, even at the magnetic field of 50 kOe. Such a linear magnetization process was ascribed to either weakened sublattice or intersublattice spins disoriented by thermal motion [35] or the noncollinear spin alignments in the magnetic system. The linear field dependence of the magnetization at higher fields is not contrary to the FIM compounds, in which strong antiferromagnetic coupling between different magnetic sublattices prevents their full alignment by the magnetic field [20]. The remanent magnetization (M_r) is 8 emu/g at 2 K, which results in a good magnetic remanence ratio (M_r/M_{50}) of ~0.6. The excellent magnetic properties may be ascribed to the quasi-one-dimensional Fe_2Se_3 double chains in the hybrid rods, which is potential to be applied in the new type of permanent magnets.

Quasi-1D spin-ladder compounds, such as $M\text{Fe}_2\text{Se}_3$ ($M = \text{Ba}, \text{Cs}$) [25–28], have attracted considerable interest. Either block magnetism [25] or stripelike magnetism [27] was proposed as the magnetic origins of these ladder compounds, where the magnetic moments couple ferromagnetically (or antiferromagnetically) along the rung (or the leg) direction. Because spin ladders in copper oxides shed light on the mechanism of superconductivity, a study on an analog with ladder geometry among ferrous compounds is highly interesting. It is obvious that all the iron atoms in BaFe_2Se_3 are ferric, while those in CsFe_2Se_3 are composed of ferric and ferrous ions with a molar ratio of 1:1. In our case, the molecular formula of $[\text{Fe}_{1.125}^{3+}\text{Fe}_{0.875}^{2+}\text{Se}_3^{2-}]_2[\text{Fe}^{2+}(\text{dien})_2]_{0.875}$ reveals the iron composition, which enables creation of a magnetic structure that is different from those for the antiferromagnetic BaFe_2Se_3 and CsFe_2Se_3 due to the varied content of ferric and ferrous ions. This monoclinic hybrid material has been classified by the large magnetization and coercivity at 2 K as a ferrimagnetic compound. In comparison with the $\text{Fe}_3\text{Se}_4(\text{dien})_2$ with 1D $\text{Fe}^{3+}\text{Se}_2^{2+}$ single chains [13], the ferric and ferrous ions in $\text{Fe}_{1.125}^{3+}\text{Fe}_{0.875}^{2+}\text{Se}_3^{2-}$ double chains should be responsible for the ferrimagnetic interactions. Moreover, we easily see that the $\text{Fe}_{1.125}^{3+}\text{Fe}_{0.875}^{2+}\text{Se}_3^{2-}$ double chains in present hybrid rods are different from $\text{Fe}_2^{3+}\text{Se}_3^{2-}$ in BaFe_2Se_3 and $\text{Fe}^{3+}\text{Fe}^{2+}\text{Se}_2^{2-}$ in CsFe_2Se_3 . Due to a diffusing reaction in the formation of $[\text{Fe}_{1.125}^{3+}\text{Fe}_{0.875}^{2+}\text{Se}_3^{2-}]_2[\text{Fe}^{2+}(\text{dien})_2]_{0.875}$, the distributions of Fe^{3+} and Fe^{2+} in the $\text{Fe}_{1.125}^{3+}\text{Fe}_{0.875}^{2+}\text{Se}_3^{2-}$ double chains are not clear. Efforts to examine the magnetic struc-

ture of $[\text{Fe}_2\text{Se}_3]_2[\text{Fe}(\text{dien})_2]_{0.9}$ hybrid rods with determined atom coordinates are currently in progress.

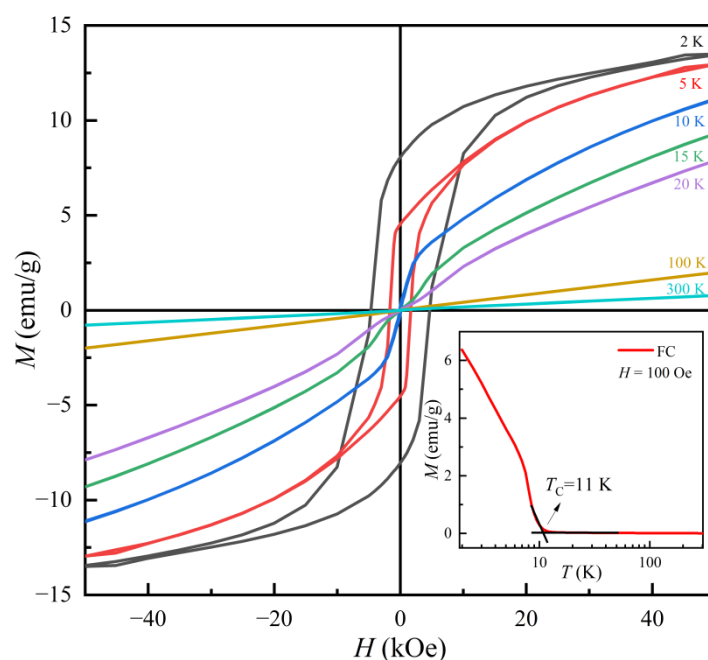


Figure 9. Hysteresis loops of $(\text{Fe}_2\text{Se}_3)_2[\text{Fe}(\text{dien})_2]_{0.9}$ hybrid rods measured at different temperatures. Inset shows temperature dependence of FC magnetizations in a magnetic field $H = 100$ Oe.

4. Conclusions

We developed a facile protocol for bottom-up synthesizing organic–inorganic hybrid materials by connecting inorganic fragments of FeSe_2 single chains, Fe_2Se_3 double chains or $\beta\text{-Fe}_x\text{Se}$ layers with $\text{Fe}(\text{dien})_2$ complexes. These materials possess varied crystal structures and magnetic properties. Of note, the monoclinic $(\text{Fe}_2\text{Se}_3)_2[\text{Fe}(\text{dien})_2]_{0.9}$ hybrid rods with the space group $P2_1/c$ (14) are ferrimagnetic and the Curie temperature (T_C) is determined to be ~ 11 K. The hybrid rods show a high coercivity (H_C) of 4.67 kOe and a saturated magnetization (M_S) of 13.5 emu/g at 2 K, which should be ascribed to the ferrimagnetic coupling between the organic $\text{Fe}(\text{dien})_2$ complexes and inorganic Fe_2Se_3 double chains. Large coercivity and magnetic remanence ratios make the monoclinic hybrid rods an excellent organic permanent magnet.

Author Contributions: Conceptualization, D.L.; methodology, D.L.; investigation, X.S., Q.K., X.M. and S.L.; formal analysis, X.S.; resources, D.L. and Z.Z.; data curation, X.S.; writing—original draft preparation, X.S. and D.L.; writing—review and editing, D.L. and Z.Z.; supervision, D.L. and Z.Z. All authors have read and agreed to the published version of the manuscript.

Funding: This research was funded by the National Natural Science Foundation of China under Grant No. 51971221, 52031014 and by the National Key R&D Program of China (No. 2017YFA0700702) from the ministry of Science and Technology of China.

Data Availability Statement: The data are available upon reasonable request from the corresponding author.

Conflicts of Interest: The authors declare no conflict of interest.

References

- Wei, M.M.; Fan, Y.C.; Qin, W. Progress of organic magnetic materials. *Sci. China Phys. Mech.* **2019**, *62*, 977501. [\[CrossRef\]](#)
- Sanchez, C.; Julian, B.; Belleville, P.; Popall, M. Applications of hybrid organic-inorganic nanocomposites. *J. Mater. Chem.* **2005**, *15*, 3559–3592.
- Welbes, L.L.; Borovik, A.S. Confinement of metal complexes within porous hosts: Development of functional materials for gas binding and catalysis. *Acc. Chem. Res.* **2005**, *38*, 765–774. [\[CrossRef\]](#)
- Ansari, F.; Ding, Y.C.; Berglund, L.A.; Dauskardt, R.H. Toward sustainable multifunctional coatings containing nanocellulose in a hybrid glass matrix. *ACS Nano* **2018**, *12*, 5495–5503. [\[CrossRef\]](#)
- Li, W.; Xia, F.; Qu, J.; Li, P.; Chen, D.H.; Chen, Z.; Yu, Y.; Lu, Y.; Caruso, R.A.; Song, W.G. Versatile inorganic-organic hybrid WO_x-ethylenediamine nanowires: Synthesis, mechanism and application in heavy metal ion adsorption and catalysis. *Nano Res.* **2014**, *7*, 903–916. [\[CrossRef\]](#)
- Jin, S.F.; Fan, X.; Wu, X.Z.; Sun, R.J.; Wu, H.; Huang, Q.Z.; Shi, C.L.; Xi, X.K.; Li, Z.L.; Chen, X.L. High-*T_C* superconducting phases in organic molecular intercalated iron selenides: Synthesis and crystal structures. *Chem. Commun.* **2017**, *53*, 9729–9732. [\[CrossRef\]](#) [\[PubMed\]](#)
- Zhao, H.Y.; Fu, H.R.; Hu, Z.; Fu, Q.M.; Tao, H.; Weng, J.; Xiong, L.W.; Cheng, Z.X. Magnetic hybrid organic-inorganic perovskite (CH₃NH₃)₂XCl₄ (X = Mn, Cu, Co) crystals. *CrystEngComm* **2021**, *23*, 5208–5213. [\[CrossRef\]](#)
- Asensio, Y.; Marras, S.; Spirito, D.; Gobbi, M.; Ipatov, M.; Casanova, F.; Mateo-Alonso, A.; Hueso, L.E.; Martin-Garcia, B. Magnetic properties of layered hybrid organic-inorganic metal-halide perovskites: Transition metal, organic cation and perovskite phase effects. *Adv. Funct. Mater.* **2022**, *32*, 2207988. [\[CrossRef\]](#)
- Kim, K.Y.; Park, G.; Cho, J.; Kim, J.; Kim, J.S.; Jung, J.; Park, K.; You, C.Y.; Oh, I.H. Intrinsic magnetic order of chemically exfoliated 2D ruddlesden-popper organic-inorganic halide perovskite ultrathin films. *Small* **2020**, *16*, 2005445. [\[CrossRef\]](#)
- Zhang, S.L.; Li, X.C.; Gu, S.Y.; Guo, S.; Liu, Z.Y.; Zeng, S.Y.; Li, S.S. Crystal structures and magnetic properties of one-dimensional compounds constructed from Mn₂(salen)₂ building blocks and organic selenite acid ligands. *N. J. Chem.* **2021**, *45*, 21599–21605. [\[CrossRef\]](#)
- Sibille, R.; Mazet, T.; Diop, L.V.B.; Francois, M. Crystal structure and magnetic properties of the layered hybrid organic-inorganic compounds M₂(OH)₂(C₁₄H₈O₄) (M = Mn, Fe). *Acta Crystallogr. Sect. B* **2021**, *77*, 801–807. [\[CrossRef\]](#)
- Gao, M.R.; Yao, W.T.; Yao, H.B.; Yu, S.H. Synthesis of unique ultrathin lamellar mesostructured CoSe₂-amine (protonated) nanobelts in a binary solution. *J. Am. Chem. Soc.* **2009**, *131*, 7486–7487. [\[CrossRef\]](#)
- Greenfield, J.T.; Pak, C.; Kamali, S.; Lee, K.; Kovnir, K. Control over connectivity and magnetism of tetrahedral FeSe₂ chains through coordination Fe-amine complexes. *Chem. Commun.* **2015**, *51*, 5355–5358. [\[CrossRef\]](#) [\[PubMed\]](#)
- Zheng, Y.Z.; Xue, W.; Zheng, S.L.; Tong, M.L.; Chen, X.M. Néel temperature enhancement by increasing the in-plane magnetic correlation in layered inorganic-organic hybrid materials. *Adv. Mater.* **2008**, *20*, 1534–1538. [\[CrossRef\]](#)
- De Luis, R.F.; Urtiaga, M.K.; Mesa, J.L.; Vidal, K.; Lezama, L.; Rojo, T.; Arriortua, M.I. Short-range and long-range magnetic ordering, in third generation brannerite type inorganic-organic-vanadates: [{Mn(Bpy)}(VO₃)₂] approximate to (H₂O)_{1.16} and [{Mn(Bpy)_{0.5}}(VO₃)₂] approximate to (H₂O)_{0.62}. *Chem. Mater.* **2010**, *22*, 5543–5553. [\[CrossRef\]](#)
- Kurmoo, M.; Kumagai, H.; Green, M.A.; Lovett, B.W.; Blundell, S.J.; Ardavan, A.; Singleton, J. Two modifications of layered cobaltous terephthalate: Crystal structures and magnetic properties. *J. Solid State Chem.* **2001**, *159*, 343–351. [\[CrossRef\]](#)
- Pak, C.; Kamali, S.; Pham, J.; Lee, K.; Greenfield, J.T.; Kovnir, K. Chemical excision of tetrahedral FeSe₂ chains from the superconductor FeSe: Synthesis, crystal structure, and magnetism of Fe₃Se₄(en)₂. *J. Am. Chem. Soc.* **2013**, *135*, 19111–19114. [\[CrossRef\]](#)
- Zang, Z.-A.; Yao, H.-B.; Zhou, Y.-X.; Yao, W.-T.; Yu, S.-H. Synthesis and magnetic properties of new [Fe₁₈S₂₅](TETAH)₁₄ (TETAH = protonated triethylenetetramine) nanoribbons: An efficient precursor to Fe₇S₈ nanowires and porous Fe₂O₃ nanorods. *Chem. Mater.* **2008**, *20*, 4749–4755. [\[CrossRef\]](#)
- Kuang, Q.; Men, X.; Shang, X.; Yang, B.; Zhou, Y.; Zhang, B.; Li, Z.; Li, D.; Zhang, Z. Magnetism of tetragonal β-Fe₃Se₄ nanoplates controllably synthesized by thermal decomposition of (β-Fe₂Se₃)₄[Fe(tepa)] hybrid. *Magnetism* **2022**, *2*, 31–44. [\[CrossRef\]](#)
- Pan, D.S.; Li, Y.; Han, Z.; Li, B.; Wang, C.W.; Yang, T.; Li, D.; Choi, C.K.; Zhang, Z.D. Organic-inorganic hybrid (β-Fe₃Se₄)₄[Fe(teta)_{1.5}] (teta = triethylenetetramine) nanoplates: Solution synthesis and magnetic properties. *Chem. Mater.* **2018**, *30*, 8975–8982. [\[CrossRef\]](#)
- Kaiba, A.; Al Otaibi, F.; Geesi, M.H.; Riadi, Y.; Aljohani, T.A.; Guionneau, P. A new organic-inorganic hybrid compound (NH₃(CH₂)₆H₄CO₂H)[SnCl₆]: Synthesis, crystal structure, vibrational, optical, magnetic properties and theoretical study. *J. Mol. Struct.* **2021**, *1234*, 130129. [\[CrossRef\]](#)
- Pan, D.S.; Kuang, Q.F.; Tong, P.; Tong, W.; Fan, L.B.; Zhao, J.; Li, D.; Choi, C.J.; Zhang, Z.D. Self-assembly of 1D FeSe₂ chains and Fe(dien)₂ complexes for ferrimagnetic inorganic-organic hybrid cuboids. *J. Magn. Magn. Mater.* **2022**, *542*, 168585. [\[CrossRef\]](#)
- Chen, T.K.; Chang, C.C.; Chang, H.H.; Fang, A.H.; Wang, C.H.; Chao, W.H.; Tseng, C.M.; Lee, Y.C.; Wu, Y.R.; Wen, M.H.; et al. Fe-vacancy order and superconductivity in tetragonal β-Fe_{1-x}Se. *Proc. Natl. Acad. Sci. USA* **2014**, *111*, 63–68. [\[CrossRef\]](#) [\[PubMed\]](#)
- Tezze, D.; Pereira, J.M.; Asensio, Y.; Ipatov, M.; Calavalle, F.; Casanova, F.; Bittner, A.M.; Ormazza, M.; Martin-Garcia, B.; Hueso, L.E.; et al. Tuning the magnetic properties of NiPS₃ through organic-ion intercalation. *Nanoscale* **2022**, *14*, 1165–1173. [\[CrossRef\]](#)

25. Nambu, Y.; Ohgushi, K.; Suzuki, S.; Du, F.; Avdeev, M.; Uwatoko, Y.; Munakata, K.; Fukazawa, H.; Chi, S.; Ueda, Y.; et al. Block magnetism coupled with local distortion in the iron-based spin-ladder compound BaFe_2Se_3 . *Phys. Rev. B* **2012**, *85*, 064413. [\[CrossRef\]](#)
26. Lei, H.; Ryu, H.; Frenkel, A.I.; Petrovic, C. Anisotropy in BaFe_2Se_3 single crystals with double chains of FeSe tetrahedra. *Phys. Rev. B* **2011**, *84*, 214511. [\[CrossRef\]](#)
27. Du, F.; Ohgushi, K.; Nambu, Y.; Kawakami, T.; Avdeev, M.; Hirata, Y.; Watanabe, Y.; Sato, T.J.; Ueda, Y. Stripelike magnetism in a mixed-valence insulating state of the Fe-based ladder compound CsFe_2Se_3 . *Phys. Rev. B* **2012**, *85*, 214436. [\[CrossRef\]](#)
28. Krzton-Maziopa, A.; Pomjakushina, E.; Pomjakushin, V.; Sheptyakov, D.; Chernyshov, D.; Svitlyk, V.; Conder, K. The synthesis, and crystal and magnetic structure of the iron selenide BaFe_2Se_3 with possible superconductivity at $T_c = 11$ K. *J. Phys. Condens. Matter* **2011**, *23*, 402201. [\[CrossRef\]](#)
29. Da Li, Q.K.; Men, X.; Zhang, B.; Shang, X.; Yang, B.; Yang, T.; Li, Z.; Zhang, Z. High-temperature superconductivity ($T_C = 42$ K) of $\text{Fe}_{1.2}[\text{Fe}(\text{tepa})]_{0.8}(\beta\text{-Fe}_3\text{Se}_4)_4$. *Research Square* **2022**. Preprint (Version 1). [\[CrossRef\]](#)
30. Hua, A.; Zhou, W.Y.; Li, Y.; Li, S.Z.; Cheng, R.F.; Yang, J.X.; Luan, J.; Wang, X.H.; Jiang, C.H.; Li, D.; et al. A novel strategy for synthesizing the large size $\text{Co}_9\text{S}_8/\text{C}$ nanosheets as anode for lithium-ion batteries with superior performance. *J. Alloys Compd.* **2022**, *895*, 162668. [\[CrossRef\]](#)
31. Pan, D.S.; Xiao, B.; Wang, Q.; Wang, H. Chemical conversion synthesis of magnetic $\text{Fe}_{1-x}\text{Co}_x$ alloy nanosheets with controlled composition. *Chem. Commun.* **2021**, *57*, 2309–2312. [\[CrossRef\]](#) [\[PubMed\]](#)
32. Yao, W.T.; Yu, S.H.; Huang, X.Y.; Jiang, J.; Zhao, L.Q.; Pan, L.; Li, J. Nanocrystals of an inorganic-organic hybrid semiconductor: Formation of uniform nanobelts of $[\text{ZnSe}](\text{diethylenetriamine})_{0.5}$ in a ternary solution. *Adv. Mater.* **2005**, *17*, 2799–2802. [\[CrossRef\]](#)
33. Zhang, M.; Shi, C.; Zhang, T.K.; Feng, M.; Chang, L.; Yao, W.T.; Yu, S.H. Mn-substituted $[\text{Zn}_{1-x}\text{Mn}_x\text{Se}](\text{DETA})_{0.5}$ ($x = 0\text{--}0.3$) inorganic-organic hybrid nanobelts: Synthesis, electron paramagnetic resonance spectroscopy, and their temperature- and pressure-dependent optical properties. *Chem. Mater.* **2009**, *21*, 5485–5490. [\[CrossRef\]](#)
34. Li, Y.; Kuang, Q.F.; Men, X.L.; Wang, S.G.; Li, D.; Choi, C.J.; Zhang, Z.D. Anisotropic growth and magnetic properties of $\alpha''\text{-Fe}_{16}\text{N}_2/\text{C}$ nanocones. *Nanomaterials* **2021**, *11*, 890. [\[CrossRef\]](#)
35. Aliev, N.G.; Guseinov, N.G.; Kerimov, I.G.; Sadykhov, R.Z.; Guseinov, D.A. Magnetic-properties of Fe_3Se_4 . *Inorg. Mater.* **1977**, *13*, 519–521.
36. Kamimura, T.; Kamigaki, K.; Hirone, T.; Sato, K. On Magnetocrystalline Anisotropy of Iron Selenide Fe_7Se_8 . *J. Phys. Soc. Jpn.* **1967**, *22*, 1235–1240. [\[CrossRef\]](#)
37. Long, G.; Zhang, H.W.; Li, D.; Sabirianov, R.; Zhang, Z.D.; Zeng, H. Magnetic anisotropy and coercivity of Fe_3Se_4 nanostructures. *Appl. Phys. Lett.* **2011**, *99*, 202103. [\[CrossRef\]](#)

Disclaimer/Publisher's Note: The statements, opinions and data contained in all publications are solely those of the individual author(s) and contributor(s) and not of MDPI and/or the editor(s). MDPI and/or the editor(s) disclaim responsibility for any injury to people or property resulting from any ideas, methods, instructions or products referred to in the content.